Resource-Efficient Technologies 3 (2017) 236–248

Contents lists available at ScienceDirect

Resource-Efficient Technologies

journal homepage: www.elsevier.com/locate/reffit

Research paper

Synthesis and characterization of novel activated carbon from Medlar seed for chromium removal: Experimental analysis and modeling with artificial neural network and support vector regression

Mostafa Solgi[a], Tahereh Najib[b], Shahyar Ahmadnejad[c], Bahram Nasernejad[b,*]

[a] Chemical Engineering Department, Babol Noshirvani University of Technology, P.O. Box 484, 4714871167 Babol, Iran
[b] Chemical Engineering Department, Amirkabir University of Technology (Tehran Polytechnic), P.O. Box 15875-4413, Tehran, Iran
[c] Electrical Engineering Department, Babol Noshirvani University of Technology, P.O. Box 15875-4413, Babol, Iran

ARTICLE INFO

Article history:
Received 4 January 2017
Revised 4 August 2017
Accepted 7 August 2017
Available online 1 September 2017

Keywords:
Activated carbon
Chromium removal
Medlar seed
Artificial neural network
Support vector regression

ABSTRACT

In this study, for the first time the activated carbon has been produced from medlar seed (Mespilus germanica) via chemical activation with KOH. The carbonization process was carried out at different temperatures of 450, 550, 650 and 750 °C. The Nitrogen adsorption-desorption, Fourier transform infrared spectroscopy (FTIR) and Field Emission Scanning Electron Microscope (FESEM) analyses were carried out on the adsorbents. The effect of operating parameters, such as pH, initial concentration of Cr(VI), adsorbent dosage and contact time were investigated. The experimental data showed better agreement with the Langmuir model and the maximum adsorption capacity was evaluated to be 200 mg/g. Kinetic studies indicated that the adsorption process follows the pseudo second-order model and the chemical reaction is the rate-limiting step. Thermodynamic parameters showed that the adsorption process could be considered a spontaneous ($\Delta G < 0$), endothermic ($\Delta H > 0$) process which leads to an increase in entropy ($\Delta S > 0$). The application of support vector machine combined with genetic algorithm (SVM-GA) and artificial neural network (ANN) was investigated to predict the percentage of chromium removal from aqueous solution using synthesized activated carbon. The comparison of correlation coefficient (R^2) related to ANN and the SVR-GA models with experimental data proved that both models were able to predict the percentage of chromium removal, by synthetic activated carbon while the SVR-GA model prediction was more accurate.

1. Introduction

Accessing clean water has become one of the major challenges today due to the industrial development and the growth of cities. Increasing disposal of wastewaters containing heavy metals by various industries such as mine extractions, metal plating, textile, metallurgy has raised a global concern in recent years [1]. Among heavy metals, Cr(VI) is considered to be one of the most dangerous metals, due to its strong oxidizing nature and the ability to pass through the cell walls which might lead to cancer or mutagenesis [2].

The methods have been applied widely to treat wastewaters containing Cr(VI), include ion exchange, membrane technology, reverse osmosis, dialysis/electrodialysis, and biosorption [3–5]. Nevertheless, few drawbacks could be considered for them, such as incomplete metal removal, low selectivity, high-energy consumption and toxic sludge or other secondary wastes produced during the treatment which require proper disposal.

Another renowned approach to removing heavy metals is adsorption process which is an effective way with advantages such as high efficiency, simplicity of design and application, being inexpensive, low sensitivity to toxic substances and avoiding the production of toxic sludge. Among different adsorbents, activated carbon has some characteristics such as highly developed porosity,

Abbreviations: qe (mg/g), adsorption capacity at equilibrium time; qe,cal (mg/g), theoretical equilibrium adsorption capacity; k1 (1/min), pseudo-first order adsorption rate constant; k2 (g/mg min), pseudo-second order adsorption rate constant; kid (g/mg min), intra-particle diffusion rate constant; C, constant indicating thickness of the boundary lay; qmax (mg/g), maximum adsorption capacity; B (L/g), Langmuir isotherm constant; n, adsorption intensity; KF (mg/g), Freundlich isotherm constant; ΔS^o (J/mol K), standard entropy change; ΔGo (kJ/mol), Gibbs free energy change; ΔHo (kJ/mol), standard enthalpy change; R (j/mol K), universal gas constant; T (K), temperature; kd (ml/g), distribution coefficient; Δq (%), normalized standard deviation.

* Corresponding author.
E-mail address: banana@aut.ac.ir (B. Nasernejad).

http://dx.doi.org/10.1016/j.reffit.2017.08.003

superb adsorption capacity and high degree of surface reactivity which make it unique [6,7]. Activated carbon could be prepared through two different processes: chemical activation and physical activation. The physical activation process is carried out in two steps which the first step is carbonization of a carbonaceous material. Afterwards, in the second step which high a temperature is required, activation of char in presence of activating agents such as CO_2 or steam takes place. In comparison, Chemical activation process is a single-step method in which carbonization and activation proceeds simultaneously. Chemical activation offers some advantages over physical activation which can be summarized as follows as: (1) chemical activation can take place at lower temperatures so it needs less energy, (2) impregnation of precursor materials with the chemical agents inhibits tar formation which results in better transformation of material to carbon, in other words carbon efficiency in chemical method is significantly higher than the physical one. Chemical activation is fairly important because the surface modification done using the impregnating technique with proper environmentally-friendly chemical materials not only will increase the adsorption capacity but will also add selectivity to carbon characteristics [8]. Lots of materials (i.e. H_2SO_4, H_3PO_4, $FeCl_3$, $ZnCl_2$) have been used as chemical agents, and although $ZnCl_2$ is widely used nowadays, it is not suitable for pharmaceutical and food industries due to the environmental issues it causes [9,10]. KOH has been known to be one of the most effective chemical agents in activated carbons production, nevertheless the only problem is the high temperature required in the process [11].

According to the multitude variety of agricultural wastes in different regions, novel and inexpensive adsorbents have been manufactured in order to be used in the industries. Various materials like olive bagasse, potato peel, soybean straw, nut shells and lots of other agricultural wastes have been applied to produce activated carbon [12–15]. Another solid waste with great potential for synthesis of activated carbon is medlar seed. The medlar (Mespilus germanica) is a pear/appleshaped fruit with brown or sometimes reddish tinged color which is varying in size (diameter: 1.5–3 cm, weight: 10–80 g). The medlar trees grow wild in different regions of Middle East especially in the north of Iran and Turkey. Nevertheless, it has recently been cultivated in large-scale because of its unique properties. The processed medlar in the form of jam, marmalade and jellies has been commercially regarded by food industries. Medicinal and healing properties of medlar are well-known. It has been used as treatment for diuretic, kidney and bladder stones. Therefore, these various consumptions and five large seeds (diameter: 1–1.25 cm) lead to produce tones of medlar core as the solid wastes every year [16].

In the recent years, in addition to finding a novel, effective and economic source of activated carbon with high adsorption capacity, prediction of the output water quality and determination of experimental optimal conditions for the removal of heavy metals from a water treatment plant has become noteworthy, due to the non-linear behavior and interaction of variables during the adsorption process, so modeling the experimental data with mathematical methods is a useful solution to overcome the problems that may occur in the industrial application. In the some recent years, artificial neural network (ANN) has been widely used for modeling of experimental data in environmental problems. An investigation of artificial neural network for modeling of Cu^{2+} adsorption from industrial leachate by pumice has been conducted by a three layer feed forward backpropagation network with 4, 8 and 4 neurons in first, second and third layers [17]. In another study the response surface methodology (RSM) and artificial neural network modeling were used to predict Cu^{2+} removal from aqueous solutions by light expended clay aggregate (LECA) [18].

Despite the fact that ANN model is a useful method for modeling of the experimental data, it has some disadvantages, such as possible problem in providing of high convergence speed, avoiding local minima, and over-fitting phenomenon, thus it lacks the generalization capability. Therefore, Support Vector Machines (SVM) based on machine learning method can be a good substitution for the ANN according to its efficacious capability in prediction and classification. Application of the SVM to solve the regression problems is called SVR which has been very successful in building nonlinear data driven models, also problems characterized by small samples, nonlinearity, high dimension space and local minima. It tries to find an optimal hyper-plane function in a high dimensional space [19,20].

To the best of our knowledge, no study has been carried out on the synthesis of activated carbon from medlar seeds, therefore in this research the novel and high performance mesoporous-activated carbon from medlar seeds was prepared through chemical activation using KOH for Cr(VI) removal from aqueous solutions. The optimal values of the parameters affecting the adsorption process of chromium by synthetic activated carbon were obtained in different experiments and experimental data was modeled using SVR-GA and ANN models. To avoid any possible errors and to obtain the best results of the adsorption process modeling, parameters influencing the method of SVR were optimized by genetic algorithm (GA). Finally, to evaluate the ability of the adsorbent to be used in industrial processes, kinetic, thermodynamic and equilibrium studies were also carried out.

2. Material and methods

2.1. Material

The Medlar seeds were supplied from a local small factory which produces jelly and jam. All the chemicals used were of analytical reagent (AR) grade and obtained from Merck (Darmstadt, Germany). The standard stock solution with a chromium concentration of 1000 ppm was obtained by dissolving 2.8286 g $K_2Cr_2O_7$ in 1000 mL of deionized water. The initial pH was adjusted using solutions of 0.1 M NaOH and 0.1 M HCL.

2.2. Preparation of activated carbon

The Medlar seeds were washed extensively with deionized water in order to remove the sugar and other impurities which were stuck to the surface. Then the seeds were dried overnight at 110 °C. Afterwards, they were crushed using a micro hammer miller and were sieved in a 40/60 mesh. The crushed seeds were agitated in KOH solution with the impregnation rate of 1:3 (mass of seed/mass of KOH) at 25 °C for 8 h. After impregnation, the samples were dried overnight at 110 °C. For carbonization of the samples a quartz reactor (5 cm i.d., 100 cm length) was utilized. The reactor was placed in a tubular furnace and heated at a constant rate of 10 °C/min and then held at different carbonization temperatures (450–750 °C) for 1 h under 300 mL/min N_2 flow. The samples were remained under N_2 flow until they reached the room temperature and then they were taken out of the reactor. The resulted activated carbon were washed with 0.5 mol/L hydrochloric acid, hot and cold deionized water, respectively, until the filtrate reached a neutral pH. Finally they were dried overnight at 110 °C in hot air oven and was kept in a desiccator. The activated carbon samples produced at 450, 550, 650 and 750 °C were named AC-4, AC-5, AC-6 and AC-7, respectively.

2.3. Characterization of samples

Measuring the amount of adsorbed nitrogen is a standard method for determining the surface area and porosity of activated carbon. The analysis was performed on the samples using

the Quantachrome Autosorb Automated Gas Sorption System at a temperature of 77 K. The nitrogen adsorption isotherms were measured based on a relative pressure (P/P_0) in a range of 0.01 to 0.995. The BET surface area was determined using the Brunauer, Emett and Teller equation and also the data from nitrogen adsorption isotherm in a relative pressure range of 0.095 to 0.3. The total pore volume was considered to be equal to the amount of nitrogen adsorbed at a relative pressure of 0.995. The micropore volume and area, and also the external area of the pores (A_{ext}) were calculated using the t-plot method. The mean pore diameter was also estimated by means of the DR method. Due to its importance in determining the structure and homogeneity or heterogeneity of the pores, pore size distribution was evaluated using the BJH (Barret,Joyner and Hallonda) method [21].

The morphology of activated carbon was observed by Field Emission Scanning Electron Microscope (FESEM) (ZIESS, ΣIGMA VP). FTIR analysis was also performed on the samples within a range of 400–4000 cm^{-1} using Thermo Nicolet spectrometer (model: NEXUS 670, USA). The C, H, N, O and S elements content in the activated carbon were determined by an elemental analyzer (Heraeus, CHN-O-RAPID). Both surface acidity and basicity were determined according to procedure followed by Foo and Hameed [22]. The pH_{PZC} value was determined by the method of Bouzid et al [23].

2.4. Batch adsorption experiment

In order to study the effect of different parameters on the adsorption of Cr(VI) onto AC-7, experiments were carried out in a batch mode. The solution volume (50 ml), the shaking speed (300 rpm) and the temperature (25 °C) were all kept unchanged during the tests. After each test the concentration of Cr(VI) inside the remaining solution was determined by inductively coupled plasma–optical emission spectrometry (ICP–OES).

The percentage removal and the adsorption capacity of Cr(VI) were calculated using the following equations:

$$R\,(\%) = \frac{(C_0 - C_e)}{C_0} \times 100 \tag{1}$$

$$q_t = (C_0 - C_t) \times \frac{V}{m} \tag{2}$$

Where C_0 (mg/L), initial concentration of Cr(VI); C_e (mg/L) equilibrium concentration of Cr(VI); C_t (mg/L), concentration of Cr(VI) at time t; V (mL), volume of Cr(VI) aqueous solution; m (g), the initial concentration of adsorbent; q_t (mg/g) represent adsorption capacity for Cr(VI) at time t.

To determine the optimum pH, solutions with an initial chromium concentration of 200 mg/L were poured into closed flasks containing 0.1 g of AC-7. The pH of these solutions were set on a rage of 1–8 and the solutions were agitated for 240 min.

In order to decide on the optimum initial dose of adsorbent, solutions with an initial concentration of 100 mg/L were poured into closed flasks. The optimum pH value for the solutions which was obtained previously was set and different initial concentrations of adsorbent (0.5–5 g/L) were added to the solutions and then the suspensions were shaken for 240 min.

The procedure carried out to establish the adsorption equilibrium time was as follows: Cr(VI) solution with an initial concentration of 50, 100 and 200 mg/L was poured into closed flasks. The pH of the solutions and the initial concentration of adsorbent were set on their optimum value and then the solutions were shaken for 10, 20, 30, 60, 120, 180, 250 and 360 min.

2.5. Artificial neural network

ANN is a mathematical approach inspired by the human neurons system has been known as a powerful machine learning method. Function approximation, pattern recognition and classification are some of common applications of neural networks in different sciences. The neural network includes an input layer, an output layer and hidden layers. Among the several structure of neural network, multi-layer feed-forward network is one the most stable structure of neural network which is learned by Back-Propagation. Variations in the structure of a neural network may be due to variations in the number of layers, the number of neurons in each layer and the transfer function of neurons in each layer. The number of neurons in the input and output layers, depending on the conditions, but the number of hidden layer neurons could change for choosing the best answer [24].

2.6. Support vector regression theory

SVM was originally developed by Vapnik in 1995 [25]. The aim of SVR method is to find a function f(x) in which the predicted response y is estimated with the model error (ε), and data with ξ violation will be eliminated by a parameter denoted by C. The following linear equation is predicted by the model:

$$f(x) = \langle w, x\rangle + b \qquad w \in R^d\ ,\ b \in R \tag{3}$$

Where, b is the bias value, w is a vector for regression coefficients and $\langle w, x\rangle$ denotes the dot product between w and x in R^d. Modeling using SVR method is in fact optimizing the risk function below:

$$R = \frac{1}{N}\sum_{i=1}^{n} L(f(x_i) - y_i) + \frac{1}{2}\|w\|^2 \tag{4}$$

$$L(f(x) - y) = \begin{Bmatrix} \|f(x) - y\| - \varepsilon, & for\ |f(x) - y|\ \ x \geq \varepsilon \\ 0, & otherwise \end{Bmatrix} \tag{5}$$

Where ε represents the radius of the tube surrounding the regression function and $y_i \in R$ is the output data. Eq. (5) is known as the ε-intensive loss function. If the predicted value is within the ε-tube, the loss is zero; otherwise, is equal to the magnitude of the difference between the predicted value and the radius ε of the tube [26]. In order to obtain a simpler model w should be optimized:

$$\text{Minimize}: \frac{1}{2}\|w\|^2 + C\sum_{i=1}^{n}(\xi + \xi_i^*) \tag{6}$$

Subject to

$$\begin{Bmatrix} y_i - \langle w, x_i\rangle - b \leq \varepsilon + \xi_i \\ \langle w, x_i\rangle + b - y_i \leq \varepsilon + \xi_i^* \\ \varepsilon,\ \xi_i,\ \xi_i^* \geq 0 \end{Bmatrix} \tag{7}$$

Where $C > 0$ is penalty factor and ξ_i and ξ_i^* are slack variables used to show the distance from actual values to the corresponding boundary values of ε-tube. The above formulae indicate that increasing ε decreases the corresponding ξ_i and ξ_i^* in the same. Dual formulation of Eqs. (6) and (7) leads to maximization optimization problem as shown by Eq. (8) [27].

$$w(\alpha_i, \alpha_i^*) = \max\left(-\frac{1}{2}\sum_{i.j=1}^{n}(\alpha_i - \alpha_i^*)(\alpha_j - \alpha_j^*)\langle x, x_i\rangle - \varepsilon\sum_{i=1}^{n}(\alpha_i + \alpha_i^*) + \sum_{i=1}^{n} y_i(\alpha_i - \alpha_i^*)\right) \tag{8}$$

Table 1
Pore characteristics of the AC samples obtained at different carbonization temperature.

Sample	$S_{BET}(m^2/g)$	$V_{total}(cc/g)$	$V_{micro}(cc/g)$	$A_{ext}(m^2/g)$	$A_{micro}(m^2/g)$	Ave D(nm)
AC-4	198.6	0.2351	0.02467	154.0	44.64	4.999
AC-5	433.5	0.4432	0.1264	205.5	228.0	3.674
AC-6	1006.0	0.7935	0.3963	287.8	718.4	2.877
AC-7	1021.0	0.6876	0.4424	218.0	802.8	2.666

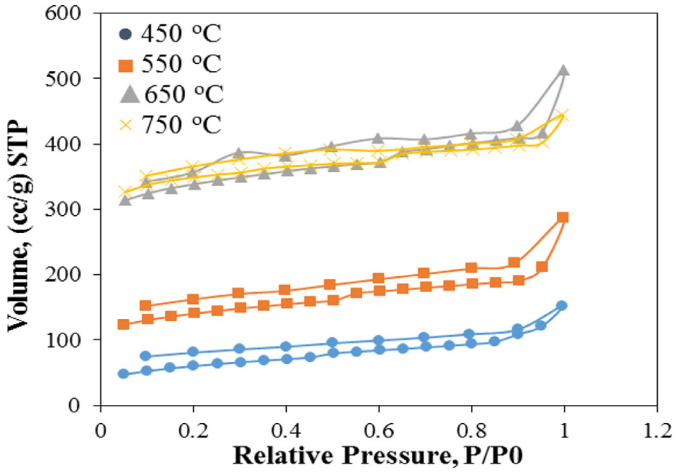

Fig. 1. N_2 adsorption–desorption isotherms of the AC samples obtained at different carbonization temperature.

Subject to

$$\sum_{i=1}^{n}\left(\alpha_i - \alpha_i^*\right) = 0 \text{ and } 0 \le \alpha_i, \alpha_i^* \le C \tag{9}$$

Where α_i and α_i^* are the Lagrangian multipliers and are gained by solving a quadratic program. As a result w calculation was performed by the following equation:

$$w = \sum_{i=1}^{l}(\alpha - \alpha_i^*)x_i \tag{10}$$

Finally, the SVR regression function is obtained in the dual space shown below:

$$f(x) = \sum_{i=1}^{n}(\alpha_i - \alpha_i^*)\langle x, x_i\rangle + b \tag{11}$$

3. Results and discussions

3.1. Characterization of activated carbon

3.1.1. N_2 adsorption-desorption isotherms

Investigation of porous structure, the size of pores and pore size distribution in a new synthesized adsorbent seems absolutely essential to realize the amount of effectiveness of the adsorbent in removing certain contaminants [28]. Fig. 1 represents nitrogen adsorption-desorption isotherms of activated carbons at different carbonization temperatures. By comparing the obtained isotherms with the IUPAC classification, the isotherms are hybrid and could be considered types I and IV, which represents carbons with microporous and mesoporous structures. At low relative pressures, due to small slope of the isotherm diagrams, the trend is basically type I with a dominant microporous structure. Although, at higher relative pressures an obvious hysteresis loop appears which reveals an adsorption behavior associated with type IV isotherms which could be associated with mesoporous structures [29]. Generally, by increasing the carbonization temperature, the adsorption capacity for nitrogen grew, nevertheless in 650 and 750 °C, no significant difference were observed and even a higher capacity for the carbon made at 650 °C, especially in relative pressure close to 1, was evaluated. Characteristics of the produced activated carbons porous structure are summarized in Table 1. Raising the temperature led to growth in the BET surface area and the microporous volume percentage. The micropore volume contributes to 64.34, 49.94, 28.52 and 10.49% of the total pore volume for AC-7, AC-6, AC-5 and AC-4, respectively. These results indicated that as the carbonization temperature rises, the structure has a tendency to become microporous. The reason is that porosity is created by KOH evaporation. Therefore because of more KOH evaporates at higher temperatures, microporosity increases [28]. Since the best porosity for Cr(VI) adsorption is provided by supermicroporous (1.5–2 nm) and small microporous materials, AC-7 was selected as the optimum activated carbon and was utilized in adsorption experiments.

Table 2
Elemental analysis of medlar seed and AC-7.

Element Name	Medlar Seed (wt %)	AC-7 (wt %)
Nitrogen	1.13	0.10
Carbon	47.93	73.12
Hydrogen	5.69	0.57
Sulphur	0.11	0.05
Oxygen[a]	45.14	26.16

[a] By difference.

3.1.2. SEM images

Fig. 2 shows the FESEM micrographs of AC-7 sample before and after adsorption, respectively. As it can be seen in Fig. 2a, an orderly and highly porous structure is achieved with a sponge-like morphology. In fact, high temperature activation has led to high porosity and omission of a substantial amount of volatile material. High porosity has provided a large surface area which also has been confirmed by BET analysis. Similar results were achieved using a different precursor and the same activation agent (KOH) by other researchers .In a study performed by Monsalvoet.al, fluffy morphology, low density and high porosity were reported for the obtained activated carbon [30]. Fig. 2b shows the AC-7 sample after the adsorption process and the white particles which have filled the surface and could not be seen in Fig. 2a represent the proper loading and adsorption of Cr(VI) ions on the adsorbent.

3.1.3. Elemental analysis

The C, H, N, O and S elements content in the raw medlar seed and AC-7 sample are given in Table 2. This table shows the high carbon content of the prepared activated carbon which justifies the suitability of the medlar seed as a precursor. The elemental analysis of medlar seed and AC-7 shows an increase in carbon level while the amount of oxygen, hydrogen, nitrogen and sulfur decreased due to the partial decomposition of volatiles compounds and degradation of organic substances in high temperature.

3.1.4. FTIR

Fig. 3 illustrate the FTIR spectrum for the AC-7 sample before and after Cr(VI) adsorption which could be used to compare

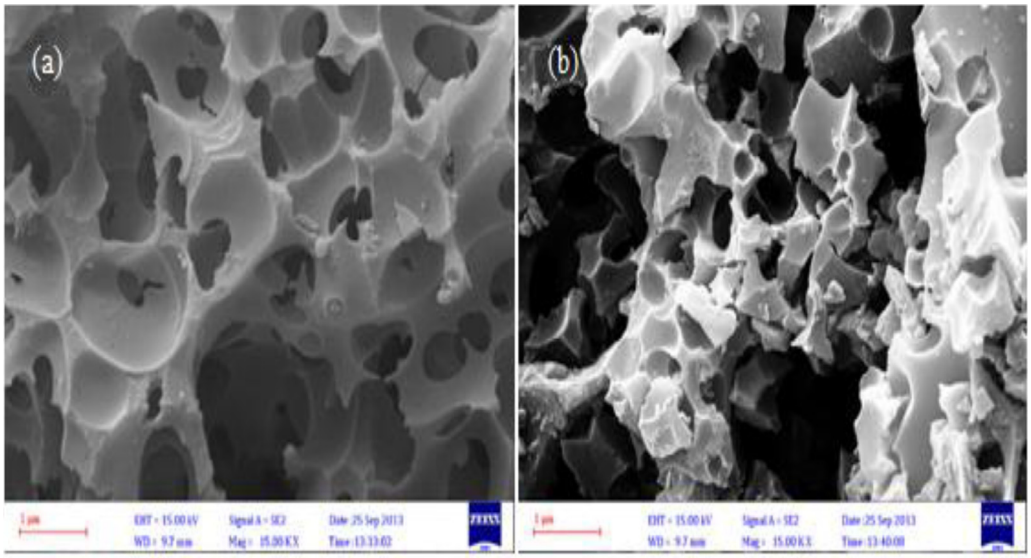

Fig. 2. FESEM micrographs of AC-7 (a) before adsorption (b) after adsorption of Cr(VI).

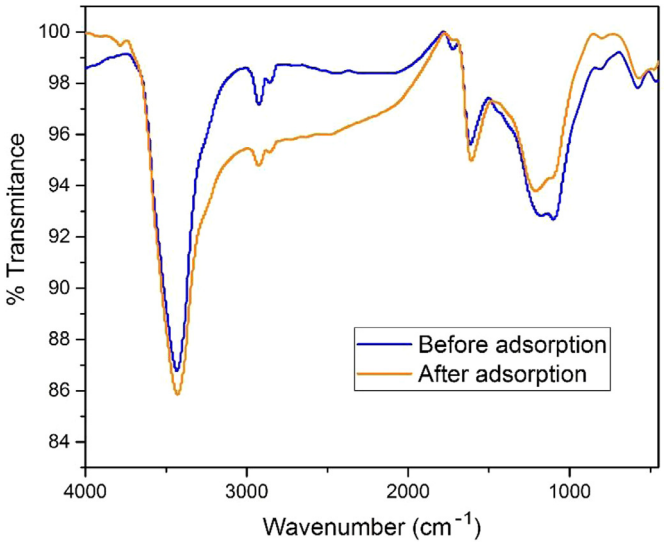

Fig. 3. FTIR spectra of AC-7 (a) before adsorption (b) after adsorption of Cr(VI).

the vibrating frequency changes for functional groups available in the adsorbent. The FTIR spectrum of activated carbon showed the following bands before adsorption: 3434.17 cm^{-1} band corresponding to O–H (hydroxyl group) stretching vibrations in alcohols, phenols and carboxylic acids and even absorbed water. Adsorption peaks observed between 2800–3000 cm^{-1} show the adsorption band for C–H group vibrations which in the present analysis, 2922.68 cm^{-1} band is obviously related to asymmetric stretching vibration of CH_2 groups and 2853.15 cm^{-1} band is related to C–H stretching vibration of aliphatic. Bands observed in 1736.22 cm^{-1} and 1621.27 cm^{-1} are corresponding to C=O stretching vibrations in carboxylic acid and N–H out-of-plane vibrations are associated with amides and amines, respectively. 1095.21 cm^{-1} and 1191.35 cm^{-1} bands are related to C–O stretching vibrations. The peak available in 585.82 cm^{-1} band shows the aromatic structure of monosustitute [31].

The FTIR spectra analysis performed after the adsorption of Cr(VI) shows some changes on the intensity and the position of peaks. The peak band of hydroxyl group was altered a little from 3434.17 cm^{-1} to 3431.50 cm^{-1}. The CH_2 stretching peak was changed from 2922.68 cm^{-1} to 2923.04 cm^{-1}. An almost complete disappearance of the peak band related to C=O in carboxylic acid in 1736.22 cm^{-1} band was noticed which indicates the complete involvement of the functional group in the adsorption process. The CH stretching peak was changed from 2853.15 cm^{-1} to 2851.89 cm^{-1}. The changing of peak band from 1621.27 cm^{-1} to 1616.89 cm^{-1} reveals the involvement of N–H group of Amines and C–O group of Amides in the adsorption process. Peaks available in 1191.35 cm^{-1} band was moved to 1212.70 cm^{-1} band and the one available in 1095.21 cm^{-1} band was moved to 1100.54 cm^{-1} band and these two changes represent the involvement of C–O group associated with chrome (VI), indeed, they prove the involvement of the functional group with the metal [32]. The peak available in 585.82 cm^{-1} band was altered to 561.83 cm^{-1} band. The changes seen in the intensity and positions of peaks indicates that Cr (VI) with functional groups available on activated carbon create some complexes and as a result confirm that adsorption process has occurred.

3.1.5. pHpzc

One of the most important characteristics of carbon adsorbents is pHpzc, which indicates the point in which the adsorbent surface charge density is zero. When the pH value of the solution is less than pHpzc the adsorbent reacts as a positively charged surface and when it is greater than pHpzc the adsorbent functions as a negatively charged surface [23]. The amount of pHpzc obtained in this research was 5.6, which shows that the ability of AC-7 in adsorbing Chromium species with negative charge in pHs lower than 5.6.

3.1.6. Surface acidity and basicity

Surface acidity and basicity is a crucial factor for describing the chemistry of carbon adsorbent surface. In the current research, the acidity and basicity of AC-7 were calculated to be 2.75 mmol/g and 0.625 mmol/g respectively. The results prove the acidity nature of AC-7 surface which is due to the presence of oxygen containing groups like carboxylic, anhydrides, lactones, phenols, while basicity could be a result of the presence of oxygen-free lewis sites, carbonyls, pyrone and chromene [22]. Observing a higher level of surface acidity than basicity for carbon adsorbent surface is in agreement with results concluded from pH_{pzc} value.

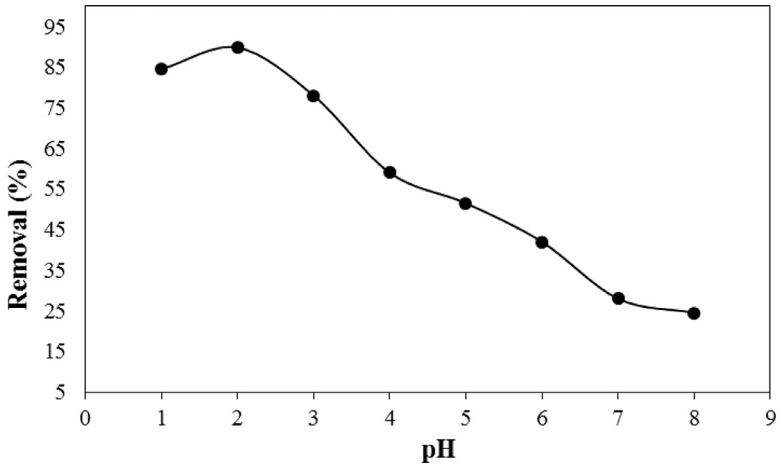

Fig. 4. The effect of pH on the adsorption of Cr(VI) onto AC-7. T = 25 °C, Time = 240 min, Ci = 200 mg/L, dose of adsorbent = 0.1 g.

3.1.7. Effect of solution pH

One of the most influential parameters on the removal of Cr(VI) is the initial pH of aqueous solution. The reason is that pH effects the various species of Cr(VI) in the solution as well as the nature of the adsorbent surface. In aqueous solutions, different species of Cr(VI), such as, H_2CrO_4, $HCr_2O_7^-$, $Cr_2O_4^-$, $Cr_2O_7^{2-}$, $HCrO_4^-$, etc. are formed. Abundance of the species in solution depends on the total concentration of Cr(VI) and the initial pH of aqueous solution. In pH values less than 1 Chromium mainly exists in form of H_2CrO_4, while in a pH range of 1–6 the dominant species of Chromium in solution is monovalent bichromate ($HCrO_4^-$) and divalent dichromate ($Cr_2O_7^{2-}$). Any further increase in pH makes $Cr_2O_4^{2-}$ the dominant specie [33].

Fig. 4 illustrates the effect of pH on the percentage removal of Cr(VI). As it can be seen in Fig. 4 in a pH range of 1 to 2 the percentage removal increases while further increase in pH up to 8 results in a dramatic decrease in percentage removal .The highest and lowest percentage removal was 89.8 and 24.5% observed at pH levels of 2 and 8, respectively. The high removal rate in acidic region could be explained by presence of anionic species of chromium and also the carbon surface charge as follows: So the electrostatic force between the negatively charged chromium species ($Cr_2O_7^{2-}$, $HCrO_4^-$) and positively charged functional groups on the adsorbent surface easily adsorbs the anions in solution. Thus, in acid regions the percentage removal is higher, however increasing pH may lead to neutral functional group on carbon adsorbent surface. Carboxylic groups on carbon surface at lower pH ($AC–COOH_2^+$) are protonated. Increasing the pH value results in subsequent formation of the neutral form ($AC(COOH)^o$) and ionized ($AC–COO^-$) which weakens the electrostatic attraction between functional groups and chromium anionic species which leads to less Cr(VI) removal [34].

3.1.8. Effect of adsorbent dosage

Fig. 5 illustrates the effect of adsorbent dosage on percentage removal and adsorption capacity of Cr(VI). As it can be seen in Fig. 5, by raising the initial concentration of adsorbent from 0.5 to 3 g/L, the percentage removal of Cr(VI) continuously grows from 77.43 to 99.9% and further increase in the initial concentration of adsorbent up to 5 g/L causes no significant changes on percentage removal of Cr(VI). The reason is that by increasing the initial concentration of adsorbent more surface area becomes accessible, and more active sites of adsorption become available for Cr(VI) ions and therefore the percentage removal obtained becomes higher. On the other hand it could be concluded from Fig. 5 that as the initial concentration of adsorbent raises from 0.5 to 5 g/L the adsorption capacity declines from 154.86 to 19.99 mg/g. The reason is that when the initial concentration of adsorbent is increased, a larger area becomes exposed to Cr(VI) ion adsorption and as a result the Cr(VI) ions face more competition to fill the actives sites and it results in lots of active sites on the surface of adsorbent to remain unsaturated and the adsorption capacity to decrease [35]. According to the obtained results a dosage of 2 g/L was selected as the optimum initial concentration of the adsorbent.

3.1.9. Effect of contact time and initial concentration on the removal of Cr(VI)

Effect of contact time and initial concentration on the removal of Cr(VI) is represented in Fig. 6. As it can be seen in Fig. 6, the adsorption process is rapid at the beginning and then it gradually slows down until an equilibrium between the adsorbent and absorbed ions is established and after that no significant change in percentage removal of Cr(VI) is observed. If the initial concentration is raised, the equilibrium time also grows in a way that for 50, 100 and 200 mg/L concentrations, the equilibrium time will be 30, 50 and 60 min, respectively. This is due to the fact that in the beginning of the process numerous vacant surface sites are available to be filled with chromium, thus the adsorption process is faster, however when lots of active sites are covered, repulsive forces between the absorbed ions and the remaining ions in the solution becomes considerable and it causes a delay in reaching the equilibrium time.

It can also be concluded from Fig. 6 that by increasing the initial concentration of Cr(VI) the removal is fallen in a way that for the initial concentrations of 50, 100 and 200 mg/L the result were observed to be 93.2, 92.1 and 89.8%. This could be explained by the fact that raising the initial concentration of the solution while the initial concentration of adsorbent is remained constant, limits the activated sites available on the adsorbent surface for metal ions and as a result the percentage removal is declined [36].

3.2. Adsorption kinetic studies

The common kinetic models to investigate the reaction pathways are including pseudo first-order, pseudo second-order, and intra-particle diffusion, which are introduced in Table 3 [37]. As it can be seen in Fig. 7a and Table 3 in different initial concentrations, the kinetic model of pseudo first order has a low correlation coefficient and there is a great difference between calculated adsorption capacity ($q_{e,cal}$) and experimental adsorption capacity ($q_{e,exp}$). On the other hand the correlation coefficient for the pseudo-second order model is very close to 1 which indi-

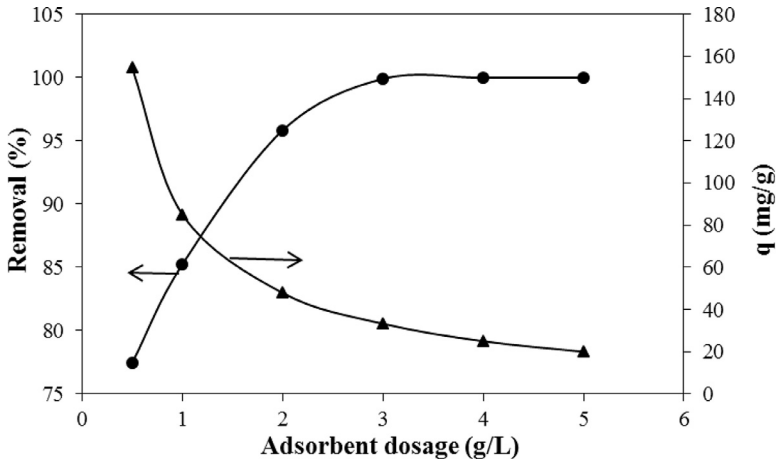

Fig. 5. Effect of the adsorbent dosage on Cr(VI) adsorption onto AC-7. T = 25 °C, Time = 240 min, Ci = 100 mg/L, pH = 2.

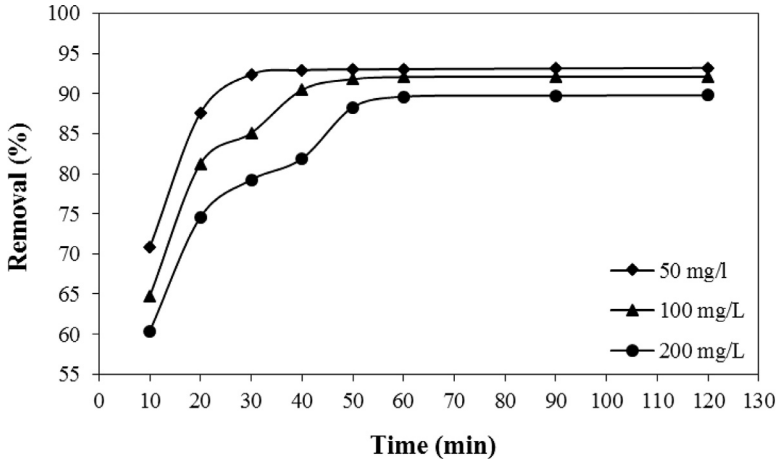

Fig. 6. Effect of contact time on the adsorption of Cr(VI) onto AC-7. T = 25 °C, dose of adsorbent 0.1 g, pH = 2.

Table 3
Kinetic parameters for the adsorption of Cr (VI) on AC-7 at different initial concentration.

Kinetics models	Parameters	C_0		
		50	100	200
Pseudo-first order $\ln(q_t - q_{e,\exp}) = \ln(q_{e,cal}) - k_1 t$	q_e (mg/g)	23.3	46.06	89.8
	K_1 (1/min)	0.038	0.048	0.03
	$q_{e,cal}$ (mg/g)	7.36	5.24	1.65
	R^2	0.93	0.93	0.8
	Δq^* (%)	25	21.5	22
Pseudo-second order $\frac{t}{q_t} = \frac{1}{k_2 q_{e,cal}^2} + \frac{1}{q_{e,cal}} t$	k_2 (g/mgmin)	0.025	0.0065	0.002
	$q_{e,cal}$ (mg/g)	23.75	47.62	94.34
	R^2	0.999	0.999	0.999
	Δq[a] (%)	5.85	4.6	2.38
Intraparticle diffusion $q_t = k_{id} t^{\frac{1}{2}} + C$	$k_{i,1}$ (mg/g (min) $^{1/2}$)	2.187	6.173	15.783
	R_1^2	0.992	0.974	0.994
	C_1	12.66	13.77	9.403
	$k_{i,2}$ (mg/g (min) $^{1/2}$)	1.053	1.901	4.13
	R_2^2	0.931	0.999	1
	C_2	17.42	32.137	0.532
	$k_{i,3}$ (mg/g (min) $^{1/2}$)	0.014	0.145	0.897
	R_3^2	0.997	0.604	0.532
	C_3	23.14	44.6	80.905

[a] $\Delta q = 100 \times \sqrt{\frac{\sum[(q_{exp} - q_{cal})/q_{exp}]^2}{n-1}}$.

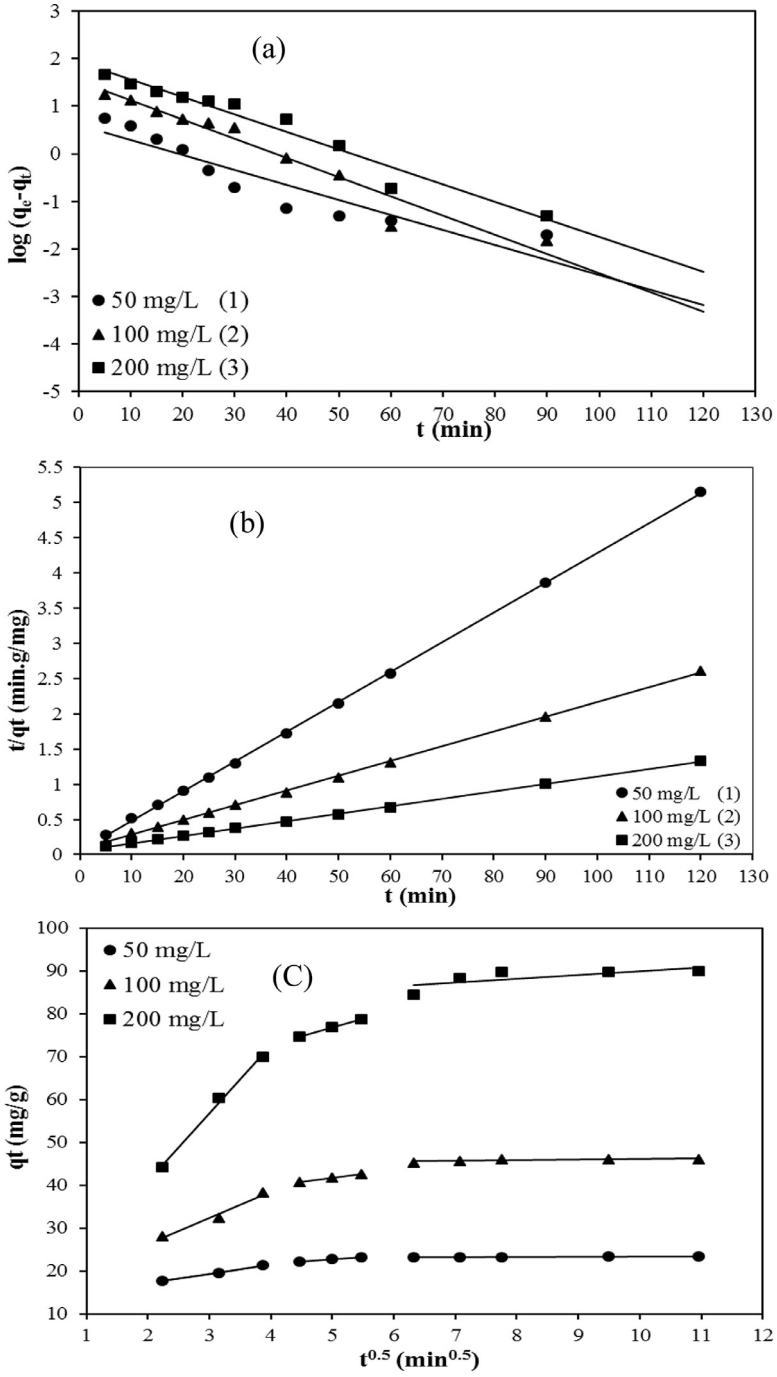

Fig. 7. Kinetic plots for adsorption of Cr(VI) onto AC-7. (a) Pseudo-first order models; (b) Pseudo-second order models; (c) intra-particle diffusion models. T = 25 °C, dose of adsorbent 0.1 g, pH = 2.

cates a very small difference between calculated adsorption capacity ($q_{e,cal}$) and experimental adsorption capacity ($q_{e,exp}$). Furthermore, the amount of $\Delta q(\%)$ related to the pseudo-second order model for three concentrations of 50, 100 and 200 mg/L seems to be at a range of 2–6% which compared to $\Delta q(\%)$ related to pseudo first order (21–25%) seems much smaller. This results also can be seen in Fig. 7b. Considering the results, it could be concluded that adsorption of Cr(VI) onto AC-7 follows the pseudo second order model and the rate limiting step may be chemical adsorption in which valance forces are involved as the result of sharing or exchanging electrons between the adsorbent and the adsorbed ions. However at the same time, the initial rapid phase may involve physical adsorption or exchange at the surface of the adsorbent. Furthermore, It can be seen in Table 3 that when the initial concentration of Cr(VI) is increased from 50 to 200 mg/L, the constant rate value of the pseudo second order model falls from 0.025 to 0.002. The reason is that when the initial concentration of Cr(VI) raises, chromium ions face more competition for being adsorbed on the adsorbents sites.

Any adsorption process on a porous adsorbent is normally controlled by three-step process. At the first step, adsorbate ions transport from bulk liquid to the boundary layer surrounding the adsorbent. Then the adsorbate ions transport from the boundary film to the external surface of the adsorbent. Finally these ions transport

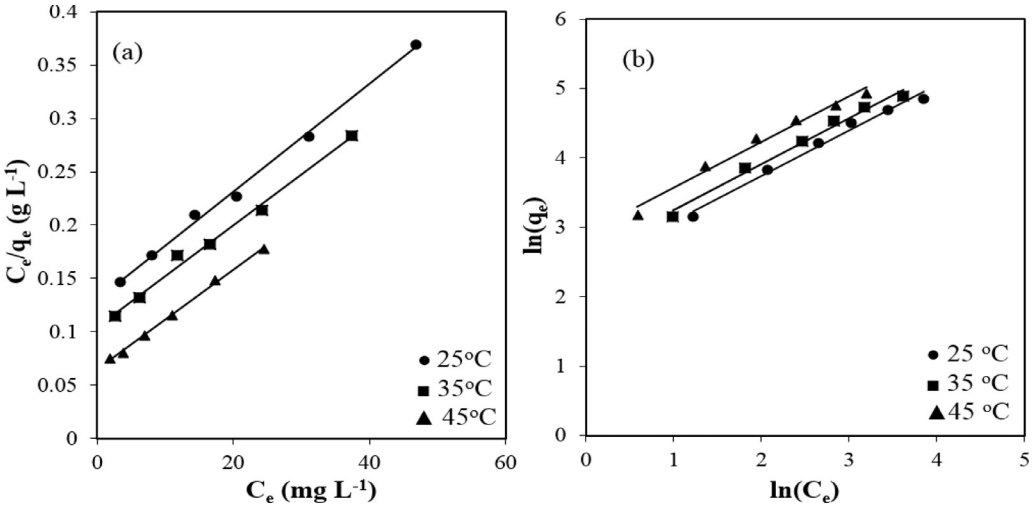

Fig. 8. Linear plots of Langmuir (a), Freundlich (b) isotherm of Cr(VI) adsorption onto AC-7.dose of adsorbent 0.1 g, pH = 2.

from the surface to the intra-particle active sites. In order to study the effect of diffusion in the adsorption kinetics, intraparticle diffusion model is applied to identify the possible rate controlling step. The plots of q_t versus $t^{1/2}$ at initial Cr(VI) concentrations of 50, 100 and 200 mg/L are depicted in Fig. 7c. According to the observation, the plot exhibited a multi-straight-line nature, suggesting that more than one process affected the adsorption. The values of k_{id} and R^2 were shown in Table 3. The data represented three periods of adsorption including the rapid section (stage 1 and stage 2) and the stabilization section (stage 3). The initial rapid stages were ascribed to the passage of Cr(VI) into the pores of AC-7 corresponding to the boundary layer diffusion. The final stage was the residual adsorption process, indicating that the adsorption reached ultimate equilibrium. Additionally, Table 3 represented that the rate constants ($k_{i,1}$, $k_{i,2}$ and $k_{i,3}$) increased significantly in all adsorption regions with increasing initial Cr(VI) concentration from 50 to 200 mg/L, suggesting that the driving force increased as the Cr(VI) concentrations was increased. These findings concluded that the adsorption of chromium onto AC-7 is a complicated process and more than one mechanism can be considered for the adsorption process [38].

3.3. Adsorption isotherm studies

In order to analyze the experimental equilibrium data, the Langmuir and Freundlich isotherm models were employed. The Langmuir isotherm model is based on three main assumptions: (i) adsorption occurs on a homogenous surface by monolayer adsorption, (ii) no interaction occurs between the adsorbed ions on the adsorbent active sites and (iii) all active sites on the surface has the same adsorption energy. An important parameter of Langmuir isotherm which provides useful information about the type of the isotherms, and feasibility of adsorption process is the dimensionless parameter R_L. If $0 < R_L < 1$ then the adsorption process is favorable, in the case of $R_L = 0$ the adsorption process is irreversible, for $R_L = 1$ the isotherm is linear and if $R_L > 1$ the adsorption process is unfavorable. On the other hand, the Freundlich isotherm model is an empirical model based on the assumption that adsorption of metal ions is a multilayer adsorption which takes place on a surface which is energetically heterogeneous. Langmuir and Freundlich isotherm constants could be obtained using the slopes and intercepts of Fig. 8a and b, respectively. The calculated parameters related to the Langmuir and Freundlich models at different temperatures are shown in Table 4. As presented in Table 4, at all temperatures the Langmuir model indicated slightly better fittings

Table 4
Langmuir and Freundlich isotherm constants for Cr(VI) adsorption onto AC-7.

Isotherm models	Parameters	Temperature (°C)		
		25	35	45
Langmuir $\frac{C_e}{q_e} = \frac{1}{b q_{max}} + \frac{C_e}{q_{max}} R_L = \frac{1}{1+bC_i}$	q_{max} (mg/g)	200	208.3	212.76
	b (L/g)	0.038	0.046	0.072
	R^2	0.997	0.991	0.998
	R_L	0.08	0.07	0.04
Freundlich $\ln q_e = \ln K_F + \frac{1}{n} \ln C_e$	n	1.52	1.5	1.51
	K_F (mg/g)	11.23	13	18
	R^2	0.984	0.987	0.981

than the Freundlich model. The maximum adsorption capacity at temperatures of 25, 35 and 45 °C by Langmuir model are found to be 200, 208.33 and 212.76 mg/g, respectively. The increase of maximum adsorption capacity with temperature shows that the bonds between the Cr(VI) ions and the active sites on the surface of the adsorbent are stronger at higher temperatures and also that the adsorption process is endothermic [40]. Furthermore, the increase in the value of b from 0.038 to 0.0725 as temperature rises proves that the process of Cr(VI) adsorption on AC-7 is endothermic. The values calculated for R_L show that the Cr(VI) adsorption process by AC-7 is favorable. The values obtained for n from the Freundlich model at different temperatures were greater than 1 which proves that the adsorption processes at the mentioned temperatures are favorable [39].

3.4. Adsorption thermodynamic studies

In order to investigate the thermodynamic behavior of the Cr(VI) adsorption onto AC-7, thermodynamic studies were conducted at different temperatures 25, 35 and 45 °C. The values for ΔH^o and ΔS^o could be obtained using the slope and intercept of the plot of $\ln k_d$ versus 1/T (Fig. 9). The values of thermodynamic parameters are given in Table 5. The negative ΔG^o values indicate that the adsorption process is thermodynamically spontaneous. In addition, Increasing ΔG^o values as the temperature raises confirms that the adsorption process is favorable at higher temperatures [40]. Considering the enthalpy values, it could be decided whether the process is a chemical adsorption or a physical one; If the enthalpy value is in a range of 2.1–20.9 kj/mol then the adsorption is a physical process, while enthalpy value is in a range of 20.9–418.4 kj/mol represent a chemical one [41]. The positive value of 26.6 kj/mol for ΔH^o in the present study shows that chemisorption

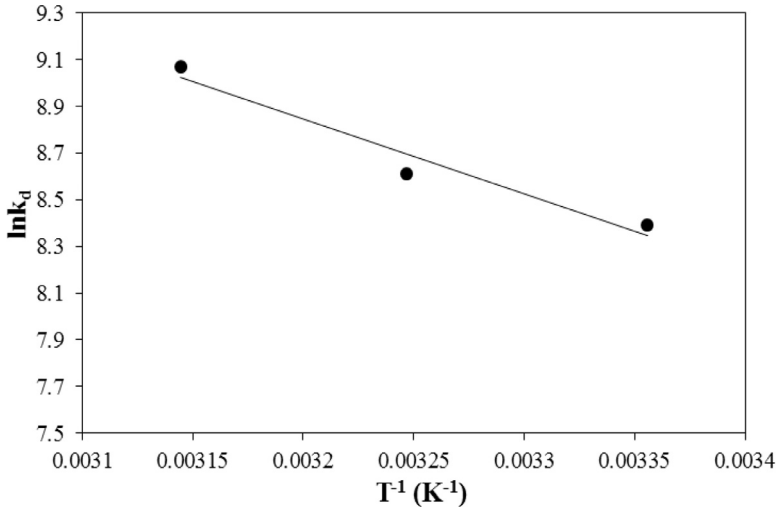

Fig. 9. Plot of LnK_d versus 1/T for Cr(VI) adsorption onto AC-7. pH = 2, dose of adsorbent 0.1 g.

Table 5
Thermodynamics parameters for Cr(VI) adsorption onto AC-7.

Thermodynamics parameters				
Thermodynamic equation	Temperature (K)	ΔG° (kJ/mol)	ΔH° (kJ/mol)	ΔS° (J/molK)
$\ln k_d = \frac{\Delta S^\circ}{R} - \frac{\Delta H^\circ}{RT}$	298	−20.8	26.6	158.7
$k_d = \frac{(C_0 - C_e)}{C_e} \times \frac{V}{m}$	308	−22	–	–
$\Delta G = -RT \ln k_d$	318	−24	–	–

may be responsible for Cr(VI) adsorption onto AC-7 which means that strong bonds between Cr(VI) ions and functional groups on the surface of the activated carbon are formed. Also the positive value of enthalpy change indicates the exothermic nature of the adsorption process whereas the positive value of ΔS° suggest an increase in the randomness at the solid/solution interface during the adsorption process.

3.5. Artificial neural network

A neural network modeling process consists of two steps; learning and testing. The obtained experimental data in this study are randomly distributed and they are classified in such way that training process will be done well. So the percentage of data which have been assigned for education and test is 70 and 30, respectively. In order to integrate the experimental data, they are normalized between 0 and 1.

$$x_i = x/x_{\max} \tag{12}$$

The regression correlation coefficient (R^2) which is used to determine the accuracy of the model defined by the following equation.

$$R^2 = \frac{\sum_N^{i=1} (x_i - x_m)^2 - \sum_N^{i=1} (x_i - y_i)^2}{\sum_N^{i=1} (x_i - y_i)^2} \tag{13}$$

In this research, the MLP network; which is a neural network for modeling nonlinear data is used. The optimum amount of weight and bias was obtained using Levenberg–Marquardt back propagation in training algorithm. The number of hidden layers and the number of neurons in hidden layers could be obtained through trial and error. Activation function (Linear Transmission) for the first layer is Logsig and for the second layer is purelin. The three-layer model was considered. The number of neurons in the first layer, the output layer and the hidden layer is 5, 1 and 8, respectively. The number of data used in this study is 59 which 41 data used for training section and 18 data used for test section. The related results to chromium removal predicted by the neural network are shown in Fig. 10. As it can be seen from this figure, in the most points the difference between experimental data and the predicted value by ANN are very slight difference. Nevertheless, in two points, 10 and 17, a considerable difference has been seen. The value of correlation coefficient of ANN was 0.958, which means this model is well able to predict the chromium removal from aqueous solution.

3.6. GA-SVR model

Eq. (11) which is usable for linear cases cannot be used for nonlinear ones. In order to overcome this limitation, the original problems must be mapped to the linear ones in a characteristic space of high dimension, in which a kernel function, $K(x_i, x_j) = \varphi(x_i)\,\varphi(x_j)$ can be used as a substitution for dot product manipulation. The typical examples of kernel function include linear, polynomial, radial basis Gaussian function (RBGF) kernels. The selection of a particular kernel function is usually needs some advance knowledge. In this study, the RBGF function, which is presented in Eq. (14), is used as the kernel function of SVR because the RBGF kernel is likely to have an acceptable performance under general smoothness assumptions [42].

$$k(x_i, x_j) = e^{-\left(\frac{(x_i - x_j)^2}{2\sigma^2}\right)} \tag{14}$$

Substituting $K(x_i, x_j) = \varphi(x_i)\,\varphi(x_j)$ in Eq. (11) gives the SVM algorithm reformulation results in a nonlinear paradigm. Thus for nonlinear cases Eq. (11) will be as follow:

$$f(x) = \sum_{i=1}^{n} (\alpha_i - \alpha_i^*) K\langle x, x_i\rangle + b \tag{15}$$

To design an effective SVR model, values of parameters in SVR have to be chosen carefully in advance. These parameters include the kernel function, regularization parameter C, variance of the

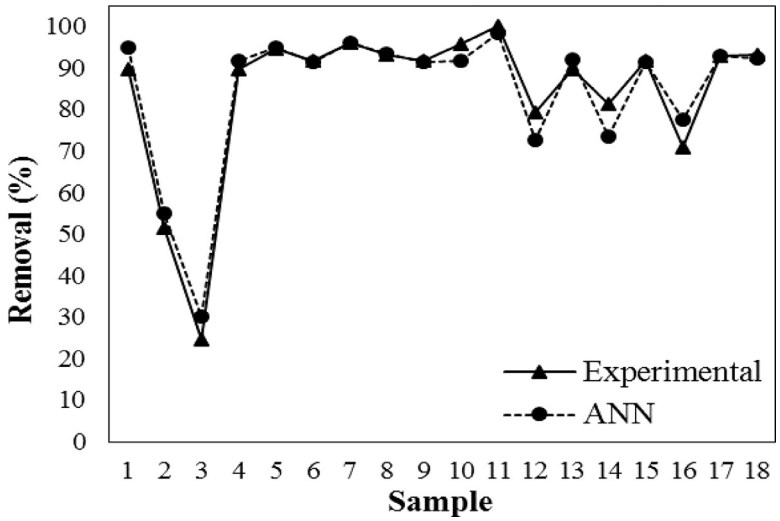

Fig. 10. Comparison between experimental data and predicted value by ANN model.

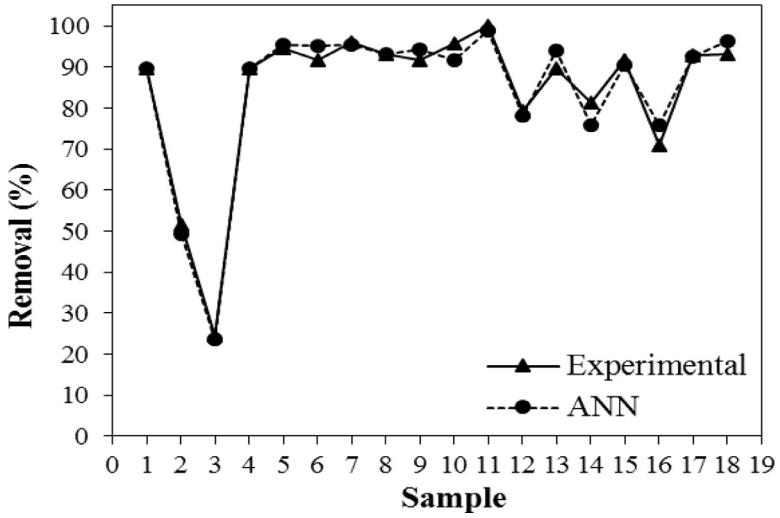

Fig. 11. Comparison between experimental data and predicted value by GA-SVR model.

kernel function (σ^2) and tube size of the ε-insensitive loss function (ε). The Genetic Algorithm (GA) is a method for selecting SVR parameters which is very prevalent among all the other popular optimization methods, due to its effectiveness in the global search of complex search spaces. GA is an evolutionary computational algorithm which performs as following: first it encodes possible solutions of the goal optimization problem by a simple chromosome-like data structure, and then sifts the critical information via some recombination operators. There operators act like the biological evolution processes such as survival of the fittest, crossover and mutation [43]. In this study the values of the SVR parameters in which calculated by GA are, 1, 3827.672 and 0.091 for σ^2, C and ε, respectively.

The predicted values of chromium removal by the GA –SVR model are shown in Fig. 11. As it can be seen in this figure, the difference between values predicted by the GA-SVR model and experimental data is minimal and in many of the points, the amount of difference is negligible. The R^2 value obtained from Eq. (13) for GA –SVR model is 0.981, which proves the fact that the GA-SVR model is able to predict the chromium removal by AC-7 more accurately.

3.7. Comparison with other adsorbent

Table 6 provides a comparison of the maximum monolayer adsorption capacity (q_{max}) obtained in the recent researches with the values reported by other researchers. The results show that the maximum adsorption capacity of AC-7 in the present work is more than all the other activated carbons obtained from different sources except Apricot stone. In general, it could be said that AC-7 could be considered as a great candidate for removing Cr(VI) from wastewaters.

4. Conclusions

Preparation of activated carbon has been attempted from Medlar seeds via chemical activation with KOH. The results of BET analysis showed that activated carbon prepared in 750 °C (AC-7) had the most surface area and the volume of micropores. Based on the conducted experiments, the optimum pH value was found to be 2 which proves that AC-7 has high level of activity in acidic regions. Furthermore, the optimum adsorbent dosage was evaluated to be 2 g/L. It was observed that the time required to reach a state of equilibrium was increased by raising the initial concentration of Cr(VI). Thus, in initial concentrations of 50, 100 and 200 mg/L the

Table 6
Comparison of the maximum adsorption capacities of chromium (VI) ions on activated carbon prepared from different sources at 25 °C.

Activated carbon Source	Activated method	pH	BET (m^2/g)	Total pore volume (cm^3/g)	q_{max} (mg/g)	Ref.
S. guttata shell	$ZnCl_2$	2	498.3	0.2322	90.9	[44]
Hazelnut shell	H_2SO_4	1	441	–	170	[45]
Peach stone	Steam air	2	608	0.341	143	[46]
Apricot stone	H_3PO_4	2	1462	0.638	212.58	[47]
Peanut shells	H_3PO_4	2	751	0.389	106.38	[48]
jatropha wood	KOH	2	1305	0.577	140.8	
Thermo-compressed fir wood slab	KOH	3	1255	0.596	180.3	[49]
pine wood	H_3PO_4		1210	0.091	124.6	
Medlar seed	KOH	2	1021	0.687	200	This study

time to reach a state of equilibrium was observed to be 30, 50, and 60 min, respectively. Kinetics studies revealed that more than one mechanism may be involved in the adsorption process. In addition, pseudo second-order kinetic model successfully fitted the experimental data and the rate-limiting step in the process might be the chemical adsorption. The equilibrium data were properly described by Langmuir model, showing a maximum adsorption capacity of 200 mg/g. Thermodynamic studies confirmed that adsorption of Cr(VI) onto AC-7 could be considered a spontaneous, endothermic, and favorable process. The dependency of chromium removal with various adsorption influential variables was well modeled using ANN and GA-SVR. The values of regression correlation coefficient for ANN ($R^2_{ANN} = 0.958$) and GA-SVR ($R^2_{SVR} = 0.981$) show that both model are well able to predict the chromium removal from aqueous solution using AC-7.

References

[1] K.V. Nimisha, A. Mohan, C. Janardhan, Pectin–Tin(IV) molybdosilicate: An ecofriendly cationic exchanger and its potential for sorption of heavy metals from aqueous solutions, Resour. Technol 2 (2016) 153–164.
[2] H. Kieu, E. Müller, H. Horn, Heavy metal removal in anaerobic semi-continuous stirred tank reactors by a consortium of sulfate-reducing bacteria, Water Res. 45 (2011) 3863–3870.
[3] L.L. Li, X.Q. Feng, R.P. Han, S.Q. Zang, G. Yang, Cr(VI) removal via anion exchange on a silver-triazolate MOF, J. Hazard. Mater. 321 (2017) 622–628.
[4] T. Riaz, A. Ahmad, S. Saleemi, M. Adrees, F. Jamshed, A.M. Hai, et al., Synthesis and characterization of polyurethane-cellulose acetate blend membrane for chromium (VI) removal, Carbohydr. Polym 153 (2016) 582–591.
[5] A. Mishra, B.D. Tripathi, A.K. Rai, Packed-bed column biosorption of chromium(VI) and nickel(II) onto Fenton modified Hydrilla verticillata dried biomass, Ecotoxicol. Environ. Saf. 132 (2016) 420–428.
[6] Y. Wu, H. Luo, H. Wang, C. Wang, Adsorption of hexavalent chromium from aqueous solutions by graphene modified with cetyltrimethylammonium bromide, Colloid Interface Sci. 394 (2013) 183–191.
[7] H. Deveci, Y. Kar, Adsorption of hexavalent chromium from aqueous solutions by bio-chars obtained during biomass pyrolysis, J. Ind. Eng. Chem 19 (2013) 190–196.
[8] A. Jain, R. Balasubramanian, M.P. Srinivasan, Hydrothermal conversion of biomass waste to activated carbon with high porosity: a review, Chem. Eng. J. 283 (2016) 789–805.
[9] O. Pezoti, A.L. Cazetta, K.C. Bedin, L.S. Souza, A.C. Martins, T.L. Silva, et al., NaOH-activated carbon of high surface area produced from guava seeds as a high–efficiency adsorbent for amoxicillin removal: Kinetic, isotherm and thermodynamic studies, Chem. Eng. J. 288 (2016) 778–788.
[10] O. Pezoti, A.L. Cazetta, I.P.A.F. Souza, K.C. Bedin, A.C. Martins, T.L. Silva, et al., Adsorption studies of methylene blue onto $ZnCl_2$-activated carbon produced from buriti shells (Mauritia flexuosa L.), J. Ind. Eng. Chem. 20 (2014) 4401–4407.
[11] K.C. Bedin, A.C. Martins, A.L. Cazetta, O. Pezoti, V.C. Almeida, KOH-activated carbon prepared from sucrose spherical carbon: Adsorption equilibrium, kinetic and thermodynamic studies for Methylene Blue removal, Chem. Eng. J. 286 (2016) 476–484.
[12] A.F. Tajar, T. Kaghazchi, M. Soleimani, Adsorption of cadmium from aqueous solutions on sulfurized activated carbon prepared from nut shells, 165 (2009) 1159–1164.
[13] J.C. Moreno-Piraján, L. Giraldo, Activated carbon obtained by pyrolysis of potato peel for the removal of heavy metal copper (II) from aqueous solutions, J. Anal. Appl. Pyrolysis. 90 (2011) 42–47.
[14] Q. Miao, Y. Tang, J. Xu, X. Liu, L. Xiao, Q. Chen, Activated carbon prepared from soybean straw for phenol adsorption, J. Taiwan Inst. Chem. Eng 44 (2013) 458–465.
[15] H. Demiral, İ. Demiral, Adsorption of chromium (VI) from aqueous solution by activated carbon derived from olive bagasse and applicability of different adsorption models, Chem. Eng. J. 15 (2008) 188–196.
[16] J. Gruz, F.A. Ayaz, H. Torun, M. Strnad, Phenolic acid content and radical scavenging activity of extracts from medlar (Mespilus germanica L) fruit at different stages of ripening, Food Chem. 124 (2011) 271–277.
[17] N.G. Turan, B. Mesci, O. Ozgonenel, The use of artificial neural networks (ANN) for modeling of adsorption of Cu(II) from industrial leachate by pumice, Chem. Eng. J. 171 (2011) 1091–1097.
[18] T. Shojaeimehr, F. Rahimpour, M.A. Khadivi, M. Sadeghi, A modeling study by response surface methodology (RSM) and artificial neural network (ANN) on Cu^{2+} adsorption optimization using light expended clay aggregate (LECA), J. Ind. Eng. Chem. 20 (2014) 870–880.
[19] S. Shokri, M.T. Sadeghi, M.A. Marvast, High reliability estimation of product quality using support vector regression and hybrid meta-heuristic algorithms, J. Taiwan Inst. Chem. Eng. 45 (2014) 2225–2232.
[20] M. Ghaedi, M. Rahimi, A.M. Ghaedi, I. Tyagi, S. Agarwal, V.K. Gupta, Application of least squares support vector regression and linear multiple regression for modeling removal of methyl orange onto tin oxide nanoparticles loaded on activated carbon and activated carbon prepared from Pistacia atlantica wood, J. Colloid Interface Sci. 461 (2015) 425–434.
[21] H. Hadoun, Z. Sadaoui, N. Souami, D. Sahel, I. Toumert, Characterization of mesoporous carbon prepared from date stems by H_3PO_4 chemical activation, Appl. Surf. Sci. 280 (2013) 1–7.
[22] K.Y. Foo, B.H. Hameed, Factors affecting the carbon yield and adsorption capability of the mangosteen peel activated carbon prepared by microwave assisted K_2CO_3 activation, Chem. Eng. J. 180 (2012) 66–74.
[23] J. Bouzid, Z. Elouear, M. Ksibi, M. Feki, A. Montiel, A study on removal characteristics of copper from aqueous solution by sewage sludge and pomace ashes, J. Hazard. Mater. 152 (2008) 838–845.
[24] M. Ghaedi, A. Daneshfar, A. Ahmadi, M.S. Momeni, Artificial neural network–genetic algorithm based optimization for the adsorption of phenol red (PR) onto gold and titanium dioxide nanoparticles loaded on activated carbon, J. Ind. Eng. Chem. 21 (2014) 587–598.
[25] V. Vapnik, The Nature of Statistical Learning Theory, Springer, New York, NY, 1995.
[26] S.K. Lahiri, K.C. Ghanta, Prediction of pressure drop of slurry flow in pipeline by hybrid support vector regression and genetic algorithm model, Chinese J. Chem. Eng. 16 (2008) 841–848.
[27] K.S. Sajan, V. Kumar, B. Tyagi, Genetic algorithm based support vector machine for on-line voltage stability monitoring, Int, J. Electr. Power Energy Syst. 73 (2015) 200–208.
[28] T.C. Chandra, M.M. Mirna, J. Sunarso, Y. Sudaryanto, S. Ismadji, Activated carbon from durian shell: Preparation and characterization, J. Taiwan Inst. Chem. Eng. 40 (2009) 457–462.
[29] S.K. Theydan, M.J. Ahmed, Adsorption of methylene blue onto biomass-based activated carbon by $FeCl_3$ activation: equilibrium, kinetics, and thermodynamic studies, J. Anal. Appl. Pyrolysis 97 (2012) 116–122.
[30] V. Monsalvo, A. Mohedano, J. Rodriguez, Activated carbons from sewage sludge: application to aqueous-phase adsorption of 4-chlorophenol, Desalination (2011).
[31] E. Kaçan, C. Kütahyali, Adsorption of strontium from aqueous solution using activated carbon produced from textile sewage sludges, J. Anal. Appl. Pyrolysis 97 (2012) 149–157.
[32] H. Zhang, Y. Tang, D. Cai, X. Liu, X. Wang, Q. Huang, et al., Hexavalent chromium removal from aqueous solution by algal bloom residue derived activated carbon: equilibrium and kinetic studies, J. Hazard. Mater. 181 (2010) 801–808.
[33] L. Zhang, Y. Tian, Y. Guo, H. Gao, H. Li, S. Yan, Introduction of α-MnO_2 nanosheets to NH_2 graphene to remove Cr^{6+} from aqueous solutions, RSC Advances 5 (2015) (2015) 44096–44106.
[34] S. Park, Y. Jang, Pore structure and surface properties of chemically modified activated carbons for adsorption mechanism and rate of Cr (VI), J. Colloid Interface Sci. (2002).
[35] L. Chabaane, S. Tahiri, a. Albizane, M. El Krati, M.L. Cervera, M. de la Guardia, Immobilization of vegetable tannins on tannery chrome shavings and their use for the removal of hexavalent chromium from contaminated water, Chem. Eng. J. 174 (2011) 310–317.

[36] M. Bilici Baskan, A. Pala, Removal of arsenic from drinking water using modified natural zeolite, Desalination 281 (2011) 396–403.
[37] Y. Ho, G. McKay, Pseudo-second order model for sorption processes, Process Biochem (1999).
[38] L. Deng, Z. Shi, X. Peng, Adsorption of Cr(VI) onto a magnetic $CoFe_2O_4$ /MgAl-LDH composite and mechanism study, RSC Adv. 5 (2015) 49791–49801.
[39] M.K. Rai, G. Shahi, V. Meena, R. Meena, S. Chakraborty, R.S. Singh, et al., Removal of hexavalent chromium Cr(VI) using activated carbon prepared from mango kernel activated with H_3PO_4, Resour. Technol. 2 (2016) S63–S70.
[40] M. Solgy, M. Taghizadeh, D. Ghoddocynejad, Adsorption of uranium(VI) from sulphate solutions using Amberlite IRA-402 resin: equilibrium, kinetics and thermodynamics study, Ann. Nucl. Energy. 75 (2015) 132–138.
[41] A. Sari, M. Tuzen, Biosorption of total chromium from aqueous solution by red algae (Ceramium virgatum): equilibrium, kinetic and thermodynamic studies, J. Hazard. Mater. 160 (2008) 349–355.
[42] Q. Li, W. Chen, Z. Liu, A. Guo, J. Huang, Nonlinear multivariable modeling of locomotive proton exchange membrane fuel cell system, Int, J. Hydrogen Energy 39 (2014) 13777–13786.
[43] W. Zhao, T. Tao, E. Zio, System reliability prediction by support vector regression with analytic selection and genetic algorithm parameters selection, Appl. Soft Comput. 30 (2015) 792–802.
[44] S. Rangabhashiyam, N. Selvaraju, Adsorptive remediation of hexavalent chromium from synthetic wastewater by a natural and $ZnCl_2$ activated Sterculia guttata shell, J. Mol. Liq. 207 (2015) 39–49.
[45] M. Kobya, Removal of Cr(VI) from aqueous solutions by adsorption onto hazelnut shell activated carbon: kinetic and equilibrium studies, Bioresour. Technol 91 (2004) 317–321.
[46] D. Duranoğlu, A.W. Trochimczuk, Ü. Beker, A comparison study of peach stone and acrylonitrile-divinylbenzene copolymer based activated carbons as chromium(VI) sorbents, Chem. Eng. J. 165 (2010) 56–63.
[47] E. Özdemir, D. Duranoğlu, Ü. Beker, A.Ö. Avcı, Process optimization for Cr(VI) adsorption onto activated carbons by experimental design, Chem. Eng. J. 172 (2011) 207–218.
[48] M. Gueye, Y. Richardson, F.T. Kafack, J. Blin, High efficiency activated carbons from African biomass residues for the removal of chromium(VI) from wastewater, J. Environ. Chem. Eng. 2 (2014) 273–281.
[49] L. Khezami, R. Capart, Removal of chromium(VI) from aqueous solution by activated carbons: kinetic and equilibrium studies, J. Hazard. Mater. 123 (2005) 223–231.